Polymerized complex and electrodeposition synthesis of Ni-doped $CuCo_2O_4$ on flexible carbon fibers as a flexible electrocatalyst for oxygen evolution reaction

Sirilak Khongthon[a, b], Sert Kiennork[b], Pakawat Wongwanwattana[b], Kittichai Sopunna[b], Anuwat Yindeesuk[c], Romteera Chueachot[a, d], Ronariddh Nakhowong [a, b, *]

[a] Functional Nanomaterials and Advanced Thermoelectric Research Laboratory, Faculty of Science, Ubon Ratchathani Rajabhat University, Ubon Ratchathani, 34000 Thailand
[b] Program of Physics, Faculty of Science, Ubon Ratchathani Rajabhat University, Ubon Ratchathani, 34000 Thailand
[c] Program of Environmental Science, Faculty of Science, Ubon Ratchathani Rajabhat University, Ubon Ratchathani,34000 Thailand
[d] Program of Chemistry, Faculty of Science, Ubon Ratchathani Rajabhat University, Ubon Ratchathani, 34000 Thailand

***Corresponding Author:** ronariddh.n@ubru.ac.th
https://doi.org/10.55674/jmsae.v11i3.251126

Received: 23 December 2022 | **Revised:** 28 December 2022 | **Accepted:** 19 July 2023 | **Available online:** 1 September 2023

Abstract

In this work, Ni-doped $CuCo_2O_4$ ($Cu_{1-x}Ni_xCo_2O_4$, x=0, 0.20, 0.40, 0.60 and 0.80) catalysts wer synthesized by polymerized complex and electrodeposition methods on flexible carbon fiber substrates for the oxygen evolution reaction (OER) in alkaline solution. The crystallinity and surface morphology of the catalysts were characterized by X-ray diffraction (XRD) and field emission scanning electron microscopy (FE-SEM).The XRD results showed that the crystallinity corresponded to $CuCo_2O_4$ phases. The OER revealed that $Cu_{0.40}Ni_{0.60}Co_2O_4$ had higher activity for OER with a low overpotential of 256 mV at a current density of 10 mA cm^{-2}, which was better than $CuCo_2O_4$ (451 mV). The results suggest that the presence of Ni^{2+} ions in spinel $CuCo_2O_4$ exhibited superior electrocatalytic activity towards OER with lower overpotential, and higher current density than $CuCo_2O_4$.

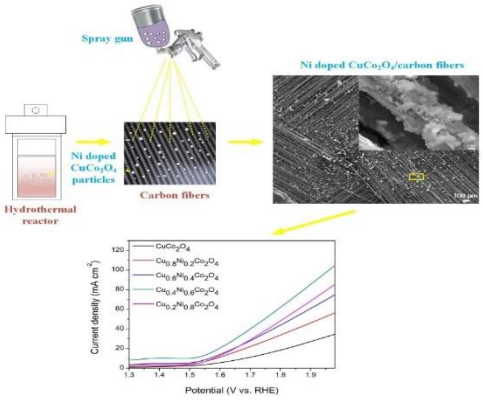

Keywords: Copper cobaltite; Nickel doping; OER; Flexible carbon fibers; Electrocatalysts; Polymerized complex method

Introduction

Water splitting is a reaction using eco-friendly technology that produces hydrogen and oxygen. It is recognized as a viable approach to enable the storage of renewable energy in the form of fuels [1]. Oxygen evolution reaction (OER) is an essential electrochemical step to convert renewable energy to storable chemical energy through the water splitting process [2]. The water splitting mechanism consists of two half-reactions. The first is a hydrogen evolution reaction (HER), which is a reduction half reaction ($2H^+ + 2e^- \rightarrow H_2$), and oxygen evolution reaction (OER), which is an oxidation half-reaction ($2H_2O \rightarrow 4H^+ + 4e^- + O_2$) [3]. However, the sluggish kinetic and complex multi-electron transfer process causes a limitation in improving the OER efficiency. Over the past decades, ruthenium oxide and Iridium oxide have shown high catalytic activity, but come with high cost and poor stability in all media [4]. Recently, copper cobaltite ($CuCo_2O_4$) was studied as an efficient OER catalyst [5, 6]. $CuCo_2O_4$ is well known for its catalytic activity towards the oxidation of CO to CO_2, alcohol synthesis, automobile pollution control, and oxygen evolution [7]. However, $CuCo_2O_4$ also exhibits relatively poor water oxidation activity and stability [6]. Many researches have been carried out to improve the efficiency of OER catalysts for $CuCo_2O_4$ by different methods. Bikkarolla et al. [5] reported that $CuCo_2O_4$ nanoparticles anchored on nitrogenated reduced graphene oxide ($CuCo_2O_4$/NrGO) exhibited minor overpotential of 0.36 V at a current density of 10 mA cm^{-2}. Du et al. [6] reported that $CuCo_2O_4$ microflowers on nickel foam exhibited low overpotential of 296 mV at a current

density of 20 mA cm^{-2}, which was better than Co_3O_4 and nickel foam. Here, we report the enhancement of Ni-doped $CuCo_2O_4$ catalysts on flexible carbon fibers prepared by the polymerized complex and electrodeposition methods. Electrochemical analysis showed that Ni-doped $CuCo_2O_4$ exhibited better OER catalysts than $CuCo_2O_4$, suggesting that Ni-doped $CuCo_2O_4$ is a promising candidate for OER catalysts.

Materials and Methods

The Ni-doped $CuCo_2O_4$ catalysts were prepared using the polymerized complex and electrodeposition methods. In a typical procedure, citric acid and ethylene glycol were mixed in the proportion of 4 and 150 moles, respectively. Subsequently, copper (II) nitrate trihydrate ($Cu(NO_3)_2 \cdot 3H_2O$, Carlo Erba) and cobalt (II) nitrate hexahydrate ($Co(NO_3)_2 \cdot 6H_2O$, Carlo Erba), and nickel nitrate hexahydrate ($Ni(NO_3)_2 \cdot 6H_2O$, Carlo Erba) according to the nominal composition of $Cu_{1-x}Ni_xCo_2O_4$ (x = 0, 0.20, 0.40, 0.60 and 0.80), were dissolved in a mixture and stirred at 200 °C for 2 h to obtain a solution. Viscous product was heated at 320 °C to burn out the versatile solvents and organic composition, resulting in a fine powder. The dark precursors were calcined at 800 °C for 6 h to obtain the crystalized $Cu_{1-x}Ni_xCo_2O_4$ phases. The obtained catalysts were coated on carbon fibers (CF). The carbon fibers (or graphite fiber) are very strong and lightweight strands of interconnected hexagonal carbon atoms or graphene sheets with about 5 – 10 µm in diameter. The excellent properties of carbon fibers such as high strength (five times higher than steel), high stiffness (2 times higher than steel), lightweight, chemical and thermal stability. The carbon fiber with a dimension of 2 × 2 cm^2 was cleaned by sonication in HCl (10%), acetone, and distilled water in sequence for 30 min each. The CF was dried at 80 °C for 2 h. The $Cu_{1-x}Ni_xCo_2O_4$ catalysts were sprayed on CF using an airbrush pen with a 0.6 mm brush nozzle. Electrodeposition method was performed using Metrohm AUTOLAB potentiostat (PGSTAT302N). The catalysts/CF were immersed in the $Cu_{1-x}Ni_xCo_2O_4$ solution with an applied potential of -1 V vs. Ag/AgCl for 10 min. Finally, the catalysts were calcined at 350 °C for 0.50 h to obtain the Ni-doped $CuCo_2O_4$/CF. Surface morphology of the catalysts was observed by field emission scanning electron microscope (FE-SEM, JOEL JSM-7610FPlus, USA). The crystalline phases of the samples were identified by X-ray diffraction (XRD, Phillips, X pert' MPD, Netherlands) using Cu*Kα* radiation (*λ*=1.5406 Å). Surface chemical compositions and valence states were carried out using X-ray photoelectron spectroscopy (XPS, AXIS ULYRA^{DLD}, Kratos Analytical, Manchester, UK) equipped with a monochromatic source (Al Kα X-rays at 1.40 keV).

Electrochemical measurement was carried out on a three-electrode system in Metrohm AUTOLAB potentiostat (PGSTAT302N). The $Cu_{1-x}Ni_xCo_2O_4$ catalysts, Pt electrode and Ag/AgCl electrode served as the working, counter, and reference electrodes, respectively. Linear sweep voltammetry (LSV) was recorded at a scan rate of 5 mV s^{-1}. Cyclic voltammetry (CV) was measured in a range from -0.1 – 0.75 V with scan rates of 5 mV s^{-1}. Cyclic voltammetry was recorded from -0.05 – 0.55 V with a scan rate of 10 to 50 mV s^{-1} in order to determine the double-layer capacitance. The double layer capacitance (C_{dl}) was determined following the relation: $j = vC_{dl}$, where j is current density and v is scan rate and C_{dl} is double layer capacitance which is slope of j versus v. Electrochemical impedance spectroscopy (EIS) measurement was performed with a frequency range from 10^5 Hz o 0.01 Hz at an AC voltage of 5 mV. All of the measurements were carried out in the 1 M KOH solution with pH 13.29. The potentials conversion from E(Ag/AgCl) to E(RHE) follows the equation: E(RHE) = E(Ag/AgCl) + 0.059*pH + 0.197 V. The overpotential (η) was calculated by using the relation: η(V) = E(RHE) – 1.23.

Results and Discussions

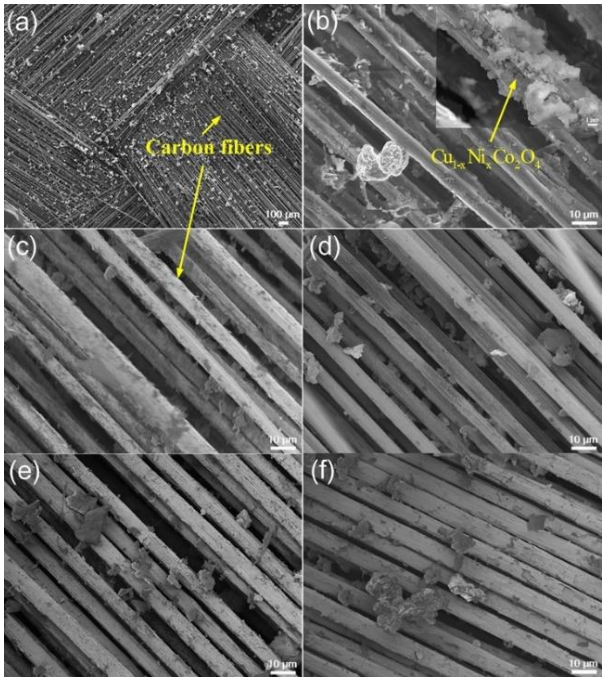

Fig. 1 FESEM images of (a) CF supported $CuCo_2O_4$, (b) $CuCo_2O_4$, (c) $Cu_{0.80}Ni_{0.20}Co_2O_4$, (d) $Cu_{0.60}Ni_{0.40}Co_2O_4$, (e) $Cu_{0.40}Ni_{0.60}Co_2O_4$, and (f) $Cu_{0.2}Ni_{0.80}Co_2O_4$.

Fig. 1 shows the morphology of the catalysts observed using FE-SEM. Fig. 1(a) shows that agglomerated particles with an average diameter range from 6 – 12 μm were dispersed on the surface of CF. FE-SEM (Fig. 1(b-f)) revealed that catalysts were dispersed on the surface of CF, while some agglomerated particles were inserted into the gap between CF. The inset figure in Fig. 1(b) shows the $CuCo_2O_4$ catalyst was coated on the CF, indicating the electrodeposition method enabled the formation of the catalyst layer on the surface of CF and helped enhance the adhesion between agglomerated particles and CF.

Elemental compositions and the valence states of the catalysts were performed by XPS. As shown in Fig. 2(a), the survey XPS spectrum shows the presence of Ni, Cu, Co, O, and C elements in the catalysts. The high-resolution XPS spectra are shown in Fig. 2 (b) – (e). The Ni 2p spectrum (Fig. 2(b)) with binding energies of 872.40 and 855.50 eV were characteristic of Ni $2p_{1/2}$ and Ni $2p_{3/2}$, respectively [8]. The Ni $2p_{3/2}$ peaks observed at 854.20, 855.50, and 856.80 eV are ascribed to Ni^{3+}, Ni^{2+}, and Ni^{2+} species, respectively [9]. Binding energies at 934.20 and 953.90 eV (Fig. 2(c)) were assigned to Cu $2p_{3/2}$ and Cu $2p_{1/2}$, respectively [10]. The deconvoluted peaks of Cu $2p_{3/2}$ at 932.60, 934.10, and 935.20 eV could be assigned to Cu^{+}, Cu^{2+}, Cu^{2+} species, respectively [5, 11]. The Co 2p spectrum (Fig. 2(d)) with binding energies at 779.50 and 795.20 eV were ascribed to Co^{2+} and Co^{3+}, respectively [10]. The Co $2p_{3/2}$ peaks were deconvoluted into three peaks located at 779.60, 780.40, and 781.90 eV corresponding to Co^{3+}, Co^{2+}, and Co^{2+} species, respectively [12, 13]. The O 1s spectrum (Fig. 2(e)) showed four peaks with binding energies at 529.80 (O1), 531.30 (O2), 532.30 (O3), and 533.50 eV (O4) assigned to metal-oxygen bonds in metal oxide, a large number of defect sites with low oxygen coordination in the materials with small particle size, and the multiplicity of physic/chemisorbed water close to the surface, respectively [6].

The XRD pattern of $Cu_{1-x}Ni_xCo_2O_4$ is shown in Fig. 3(a). Diffraction peaks at 31.23°, 36.97°, 39.03°, 59.45°, and 65.33° indexed to the (220), (311), (222), (400), (511), and (440) planes of $CuCo_2O_4$ (JCPDS no. 01-1155), respectively. The XRD peaks at 35.74°(002), 42.95°(200) corresponded to CuO and NiO, respectively while a broad peak at 26° originated from CCF. The performance of OER electrochemical catalysts was evaluated using a typical three-electrode cell setup at a scan rate of 5 mV s^{-1}. The LSV of $Cu_{1-x}Ni_xCo_2O_4$ is shown in Fig. 3(b). The $Cu_{0.40}Ni_{0.60}Co_2O_4$ catalyst exhibited higher catalytic activity than $Cu_{0.20}Ni_{0.80}Co_2O_4$, $Cu_{0.60}Ni_{0.40}Co_2O_4$, $Cu_{0.80}Ni_{0.20}Co_2O_4$, and $CuCo_2O_4$. The values for the overpotential and Tafel slope are displayed in Table 1. Values of the overpotential of the catalysts required to drive anodic current densities of 10 mA cm^{-2} of $Cu_{0.40}Ni_{0.60}Co_2O_4$ of 256 mV were lower than $Cu_{0.20}Ni_{0.80}Co_2O_4$ (351 mV), $Cu_{0.60}Ni_{0.40}Co_2O_4$ (336 mV), $Cu_{0.80}Ni_{0.20}Co_2O_4$ (358 mV), and $CuCo_2O_4$ (451 mV). The oxidation peak of $Cu_{1-x}Ni_xCo_2O_4$ prior to the onset of water oxidation was attributed to the transition of Co^{2+} to Co^{3+} or Ni^{2+} to Ni^{3+} [6]. The results exhibited Ni doping in $CuCo_2O_4$ could decrease the overpotential and cause higher current densities than $CuCo_2O_4$, which enhances electron transfer during the OER process. Tafel slopes of the catalysts were investigated to assess the OER reaction kinetics as shown in Fig. 3(c). Tafel slopes were fitted following equation: $\eta = b*\log j$, where η, b, and j denote overpotential, Tafel slope, and current density, respectively [6]. The $Cu_{0.40}Ni_{0.60}Co_2O_4$ catalyst exhibits Tafel slope of 27 mV dec^{-1}, which is lower than $Cu_{0.20}Ni_{0.80}Co_2O_4$ (37.70 mV dec^{-1}), $Cu_{0.60}Ni_{0.40}Co_2O_4$ (38.40 mV dec^{-1}), $Cu_{0.80}Ni_{0.20}Co_2O_4$ (40.2 mV dec^{-1}), and $CuCo_2O_4$ (49.9 mV dec^{-1}). The small Tafel slope of catalysts exhibits higher catalytic activity and electrocatalytic reaction rate. The typical long-term durability of $Cu_{0.40}Ni_{0.60}Co_2O_4$ is shown in Fig. 3(d). The $Cu_{0.40}Ni_{0.60}Co_2O_4$ catalyst showed good stability for OER after 8 h. The current density of $Cu_{0.40}Ni_{0.60}Co_2O_4$ catalysts suddenly decreased from 3.6 to 1.1 mA cm^{-2} and then further constant reached 8 h.

Fig. 4(a) – (b) shows the cyclic voltammetry (CV) measurement for the catalysts at different scan rates. The shapes of the CV curves (Fig. 4(a)) indicate the pseudocapacitive behavior arising from the Faradaic reaction of the Ni^{3+}/Ni^{2+} and Co^{4+}/Co^{3+} redox pairs occurred at the electrode surface [14, 15]. The $Cu_{0.40}Ni_{0.60}Co_2O_4$ showed the largest enclosed area, indicating the $Cu_{0.40}Ni_{0.60}Co_2O_4$ catalyst had higher chemical reactivity. The CV curves of Ni-doped $CuCo_2O_4$ demonstrate a large pair of redox couples ($Ni^{2+}/Ni^{3+}/Ni^{4+}$ and $Co^{2+}/Co^{3+}/Co^{4+}$) [16]. The anodic peaks of $Cu_{0.40}Ni_{0.60}Co_2O_4$ catalyst at 0.83 V and 1.67 V were ascribed to Ni^{3+}/Ni^{2+} and Ni^{3+}, Ni^{4+}/Co^{3+}, Co^{4+} transition, respectively [17, 18]. It is well known that the redox peaks of $CuCo_2O_4$ occur due to Co^{4+}/Co^{3+} redox couples [17]. Therefore, the presence of Ni^{2+} in $CuCo_2O_4$ catalyst can enhance OER activity. The anodic peaks in the CV curves shifted to a more positive potential with increased Ni doping in $CuCu_2O_4$. Fig. 4(b) shows the CV curves of $Cu_{0.4}Ni_{0.6}Co_2O_4$ electrode at a scan rate ranging from 10 – 50 mV s^{-1}. These curves are symmetric, indicating that the catalysts have a good electrochemical capacitive characteristic and superior reversible redox reaction [19].

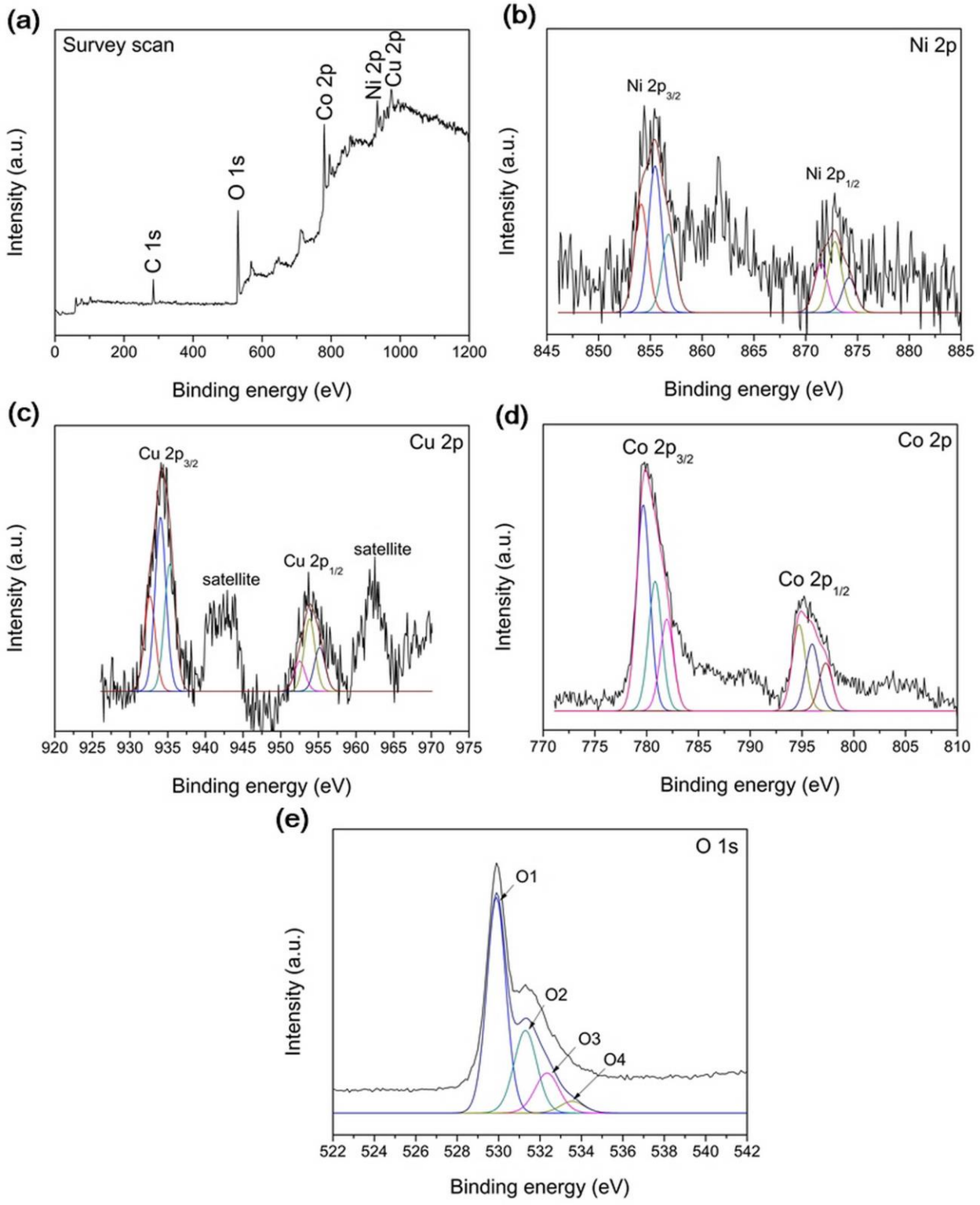

Fig. 2 X-ray photoelectron spectra of $Cu_{0.4}Ni_{0.6}Co_2O_4$: (a) survey scan, (b) Ni 2p, (c) Cu 2p, (d) Co 2p, and (e) O 1s.

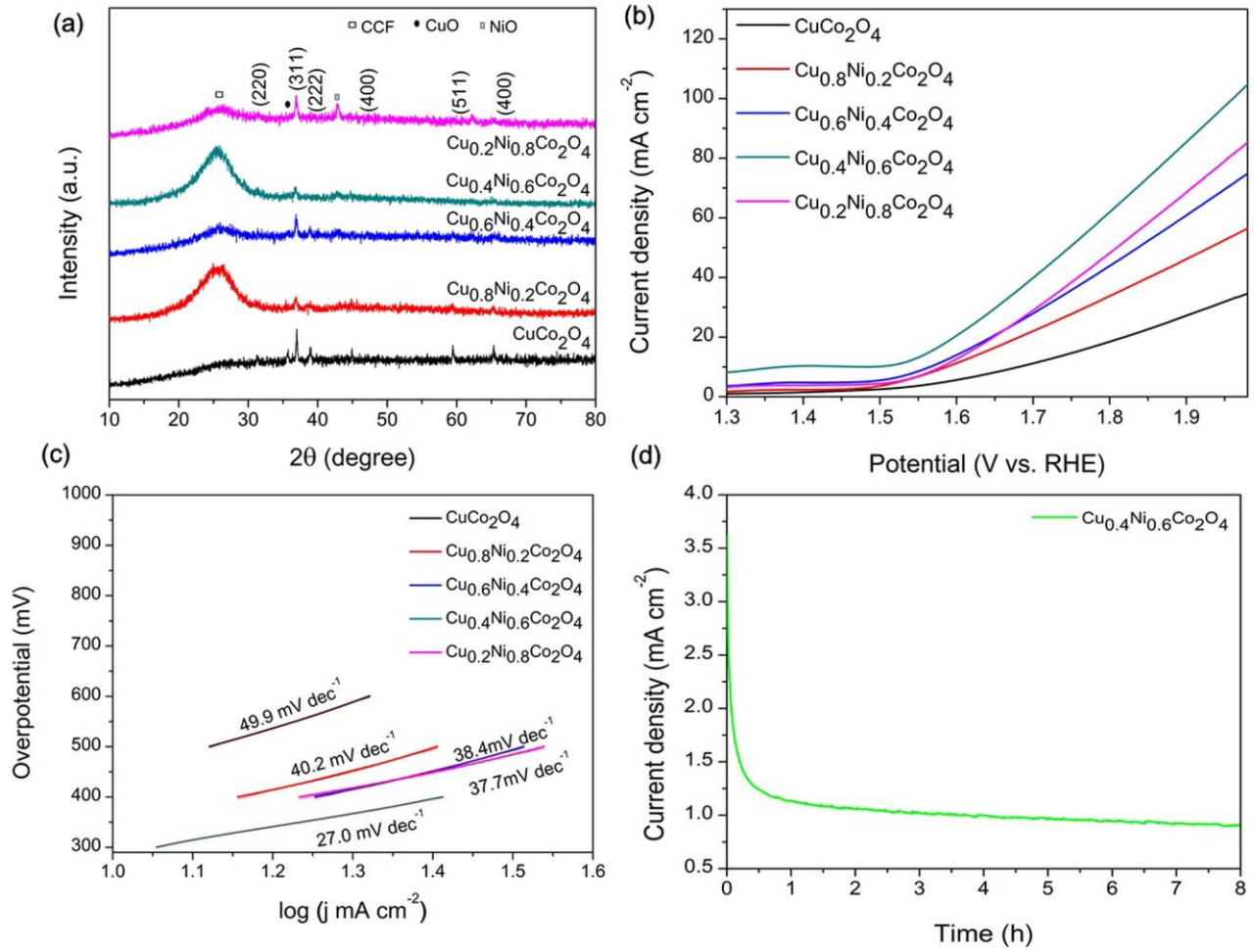

Fig. 3 (a) The XRD patterns of $Cu_{1-x}Ni_xCo_2O_4$. (b) Polarization curves and (c) Tafel plots of $Cu_{1-x}Ni_xCo_2O_4$ catalysts. (d) Chronoamperometry curve of $Cu_{0.4}Ni_{0.6}Co_2O_4$.

It is clear that the area of the current peaks in the catalysts was increased gradually as scan rate increased, indicating improved mass transportation, relatively low resistance of the electrode materials and good electrochemical reversibility [14].

Table 1 Comparison of the OER activities of $Cu_{1-x}Ni_xCo_2O_4$ (x = 0, 0.20, 0.40, 0.60 and 0.80).

Catalyst	Overpotential at 10 mA cm^{-2} (mV vs. RHE)	Tafel slope (mV dec^{-1})
$CuCo_2O_4$	451	49.90
$Cu_{0.80}Ni_{0.20}Co_2O_4$	358	40.20
$Cu_{0.60}Ni_{0.40}Co_2O_4$	336	38.40
$Cu_{0.40}Ni_{0.60}Co_2O_4$	256	27
$Cu_{0.20}Ni_{0.80}Co_2O_4$	351	37.70

The C_{dl} is used to compare the number of catalytically active sites present on the OER catalyst and electrochemically accessible surface area. Typical C_{dl} of the catalysts is shown in Fig. 4(c). The C_{dl} value of $Cu_{0.40}Ni_{0.60}Co_2O_4$ was 410 mF cm^{-2}, which was higher than $CuCo_2O_4$ (50 mF cm^{-2}). The results showed that Ni-doped $CuCo_2O_4$ catalysts exhibited higher active sites and greater surface area than $CuCo_2O_4$, indicating high electrocatalytic performance for OER [20]. EIS was carried out to further understand the reasons for the superior electrochemical performance of the catalyst. As shown in Fig. 4(d) for Nyquist plots, all catalyst electrodes showed a small real axis intercept and negligible semicircle [21]. The sloped portion of the Nyquist plots at low frequency is attributed to the Warburg resistance deriving from the frequency dependence of ion diffusion and transport in electrolyte solution [21].

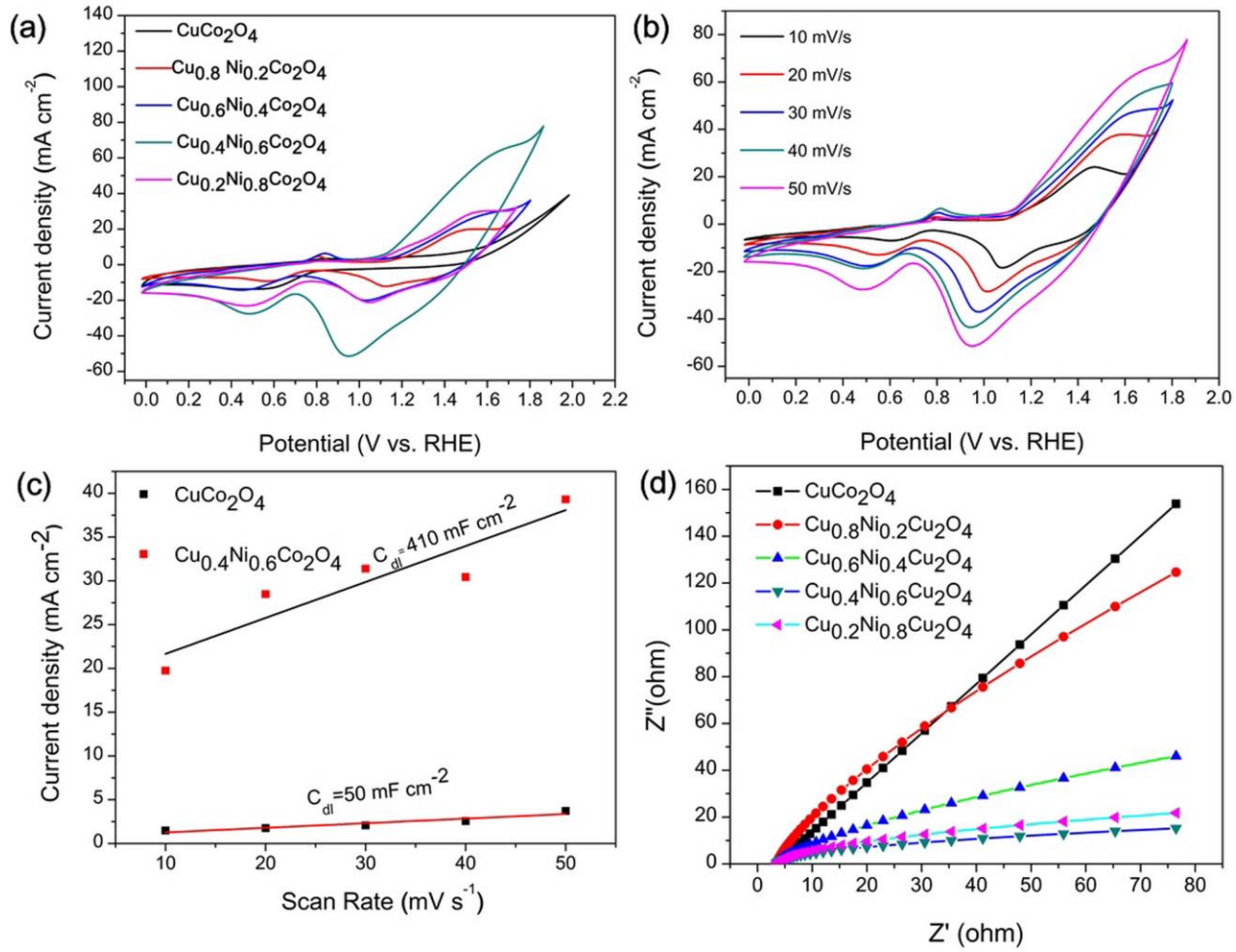

Fig. 4 (a) Cyclic voltammogram curves at scan rate 5 mV s^{-1}, (b) cyclic voltammogram in the double layer region with different scan rates (10 – 50 mV $s^{-}1$), (c) typical double-layered capacitance measurements linear fitting of the capacitive currents of the catalysts against the scan rate to fit a linear regression, and (d) Nyquist plots of $Cu_{1-x}Ni_xCo_2O_4$.

The results indicate that there is low interfacial resistance between the current collector and active materials, active materials resistance, and electrolyte resistance, as well as low charge transfer resistance [14]. The Ni-doped $CuCo_2O_4$ catalysts exhibited a relative sloping line at a low-frequency range, indicating the lower diffusive resistance and good capacitive behavior of the electrode during OER [22].

Conclusion

In summary, Ni-doped $CuCo_2O_4$ catalysts on carbon fibers were successfully synthesized using the polymerized complex and electrochemical methods. Ni-doped $CuCo_2O_4$ exhibits superior electrocatalytic activity towards OER processes with a low potential of 256 mV at a current density of 10 mA cm^{-2}, high double-layered capacitance, and high current density compared to pristine $CuCo_2O_4$. The results showed that Ni-doped $CuCo_2O_4$ catalysts could improve the active sites in the catalysts and was highly capable for use in water oxidation and energy conversion technologies.

Acknowledgement

This work was financially supported by Program of Physics, Faculty of Science, Ubon Ratchathani Rajabhat University, Thailand.

References

[1] V. D. Palma, G. Zafeiropoulos, T. Goldsweer, W. M. M. Kessels, MCM. Sanden, M. Creatore, M.N. Tsampas, Atomic layer deposition of cobalt phosphate

thin films for the oxygen evolution reaction, Electrochem. Commun. 98 (2019) 73 – 77.

[2] A. Singh, R. Yadav, G. Kociok-Köhn, M. Trivedi, U.P. Azad, A. K. Singh, A. Kumar, Syntheses of nickel sulfides from 1,2-bis(diphenylphosphino)ethane nickel(II)dithiolates and their application in the oxygen evolution reaction, Int. J. Hydrogen Energy. 43 (2018) 5985 – 5995.

[3] N. N. Som, V. Mankad, P. K. Jha, Hydrogen evolution reaction: The role of arsenene nanosheet and dopant, Int. J. hydrogen energy 43 (2018) 21634 – 21641.

[4] A. Eftekhari, Tuning the electrocatalysts for oxygen evolution reaction, Mater. today energy 5 (2017) 37 – 57.

[5] S. K. Bikkarolla, P. Papakonstantinou, $CuCo_2O_4$ nanoparticles on nitrogenated graphene as highly efficient oxygen evolution catalyst, J. Power Sources 281 (2015) 243 – 251.

[6] X. Du, X. Zhang, Z. Xu, Z. Yang, Y. Gong, $CuCo_2O_4$ microflowers catalyst with oxygen evolution activity comparable to that of noble metal, Int. J. hydrogen energy 43 (2018) 5012 – 5018.

[7] B. Chi, H. Lin, J. Li, Cations distribution of $Cu_xCo_{3-x}O_4$ and its electrocatalytic activities for oxygen evolution reaction, Int. J. hydrogen energy 33 (2008) 4763 – 4768.

[8] S. T. Senthilkumar, N. Fu, Y. Liu, Y. Wang, L. Zhou, H. Huang, Flexible fiber hybrid supercapacitor with $NiCo_2O_4$ nanograss@carbon fiber and bio-waste derived high surface area porous carbon, Electrochim. Acta 211 (2016) 411 – 419.

[9] G. Yang, S. J. Park, Facile hydrothermal synthesis of $NiCo_2O_4$- decorated filter carbon as electrodes for high performance asymmetric supercapacitors, Electrochim. Acta 285 (2018) 405 – 414.

[10] P. X. Wang, L. Shao, N. Q. Zhang, K. N. Sun, Mesoporous $CuCo_2O_4$ nanoparticles as an efficient cathode catalyst for Li-O_2 batteries, J. Power Sources 25 (2016) 506 – 512.

[11] P. Li, W. Sun, Q. Yu, P. Yang, J. Qiao, Z. Wang, D. Rooney, K. Sun, An effective three-dimensional ordered mesoporous $CuCo_2O_4$ as electrocatalyst for Li-O_2 batteries, Solid State Ion. 289 (2016) 17 – 22.

[12] L. Fang, Z. Jiang, H. Xu, L. Liu, Y. Guan, X. Gu, Y. Wang, Crystal-plane engineering of $NiCo_2O_4$ electrocatalysts towards efficient overall water splitting, J. Catal. 357 (2018) 238 – 246.

[13] S. Vijayakumar, S. Nagamuthu, K. S. Ryu, $CuCo_2O_4$ flowers/Ni-foam architecture as a battery type positive electrode for high performance hybrid supercapacitor applications, Electrochim. Acta. 238 (2017) 99 – 106.

[14] Y. Zhu, X. Ji, Z. Wu, W. Song, H. Hou, Z. Wu, X. He, Q. Chen, C. E. Banks, Spinel $NiCo_2O_4$ for use as a high-performance supercapacitor electrode material: Understanding of its electrochemical properties, J. Power Sources. 267 (2014) 888 – 900.

[15] A. Pendashteh, S.E. Moosavifard, M.S. Rahmanifar, Y. Wang, M. F. El-Kady, R. B. Kaner, M.F. Mousavi, Highly Ordered Mesoporous $CuCo_2O_4$ Nanowires, a Promising Solution for High-Performance Supercapacitors, Chem. Mater. 27 (2015) 3919 – 3926.

[16] Y. Z. Su, Q. Z. Xu, G. F. Chen, H. Cheng, N. Li, Z. Q. Liu, One dimensionally spinel $NiCo_2O_4$ nanowire arrays: facile synthesis, water oxidation, and magnetic properties, Electrochim. Acta. 174 (2015) 1216 – 1224.

[17] S. Cui, S. Gu, Y. Ding, J. Zhang, Z. Zhang, Z. Hu. Hollow mesoporous $CuCo_2O_4$ microspheres derived from metal organic framework: A novel functional materials for simultaneous H_2O_2 biosensing and glucose biofuel cell, Talanta. 178 (2018) 788 – 95.

[18] J. Wang, T. Qiu, X. Chen, Y. Lu, W. Yang, Hierarchical hollow urchin-like $NiCo_2O_4$ nanomaterial as electrocatalyst for oxygen evolution reaction in alkaline medium, J. Power Sources 268 (2014) 341 – 348.

[19] L. Huang, D. Chen, Y. Ding, S. Feng, Z.L. Wang, M. Liu, Nickel−cobalt hydroxide nanosheets coated on $NiCo_2O_4$ nanowires grown on carbon fiber paper for high-performance pseudocapacitors, Nano Lett. 13 (2013) 3135 – 3139.

[20] H. A. Bandal, A. R. Jadhav, H. Kim, Facile synthesis of bicontinuous Ni_3Fe alloy for efficient electrocatalytic oxygen evolution reaction, J. Alloys Compd. 726 (2017) 875 – 884.

[21] P. Liang, F. Wang, Z. A. Hu, Controlled synthesis of ordered sandwich $CuCo2O_4$/reduced graphene oxide composites via layer-by-layer heteroassembly for high-performance supercapacitors, Chem. Eng. J. 350 (2018) 627 – 636.

[22] Y. Zhang, J. Wang, J. Ye, P. Wan, H. Wei, S. Zhao, T. Li, S. Hussain, $NiCo_2O_4$ arrays nanostructures on nickel foam: Morphology control and application for pseudocapacitors, Ceram. Int. 42 (2016) 14976 – 14983.